# Nanoscale

Accepted Manuscript


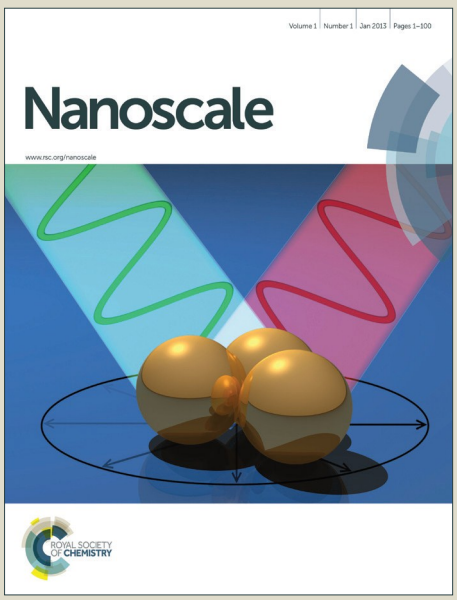





ROYAL SOCIETY OF CHEMISTRY

www.rsc.org/nanoscale

Journal Name

ARTICLE

# A New Approach to Understand Cassie State of Liquids on Superamphiphobic Materials

Received 00th January 20xx,
Accepted 00th January 20xx

DOI: 10.1039/x0xx00000x

www.rsc.org/

Tao Wang, Jing Cui, Shenshen Ouyang, Weihao Cui and Sheng Wang*

Hierarchical structure is a prerequisite for liquid super-repellent surface due to its capability to catch large numbers of fine air-pockets. In the present work, a series of hierarchical nanocomposites with anti-wettability were fabricated by in-situ deposition of spherical $SiO_2$ nanoparticles on Te@C nanofibers. $N_2$ adsorption-desorption isotherms were used for the first time to characterize the air-pockets and relate them to the wettabilty of the nanocomposites. The results indicate that superamphiphobicity is a contribution of delicate synergistic effect between micro-scale structure and nano-scale structure. Significant dominance of either of them led to reduced superamphiphobicity. The superamphiphobic "beads on a string" materials should meet the following features: higher $S_{BET}$ that ensures enough air-pockets ($S_{BET}$ value of superamphiphobic sample is much higher than that of superhydrophobic one); and the most important, a "continuous and balanced" distribution of micro and macro air-pockets derived from hierarchical structure

## Introduction

Based on the discovery and extensive exploration of "lotus effect" by Barthlott and Neinhuis,[1,2] fabrication and characterization of superhydrophobic materials (water contact angle is greater than 150° with sliding angle less than 5°) by biomimetic approach has become one of the hottest research topics.[3-6] It has been demonstrated that the surface architecture of hierarchical structures combined with low surface energy materials is the key factor to achieve superhydrophobicity.[7,8] Superamphiphobicity (contact angles of water and oil > 150° with sliding angles less than 5°) is a new concept derived from previous research findings of superhydrophobicity.[9-14] However, fabrication of a superamphiphobic surface is much more difficult than that of superhydrophobic one due to the lower surface energy of organic liquids than that of water. For example, the surface energy ($\gamma_{lv}$) of water is 72.1 mN/m and those of olive oil and *n*-hexadecane only are 32.0 mN/m and 27.5 mN/m, respectively. Therefore, the organic liquids can readily spread on many solid substrates.

Several artificial superamphiphobic surfaces have been successfully fabricated. The fabrication processes indicate that, first, superamphiphobicity cannot be achieved on flat substrate even it is modified with the lowest surface energy material such as fluorinated decyl polyhedral oligomeric silsesquioxanes (FD-POSS, $\gamma_{SV}$ = 10 mN/m).[10,15] Second, it is much easier to obtain superamphiphobicity on a well-defined topography even it is only modified with common fluorination materials.[16-18] Therefore, hierarchical surface structure should be the most important factor for creating a superamphiphobic surface. For example, in addition to the secreted wax, the special hierarchical structure of water strider legs plays an important role on remarkable non-wetting property. This is attributed to the fine nanogrooves of the hierarchical structure.[19] Hierarchical structures contain textures with multiple length scales can much more effectively trap the air than a single scale texture do.[20,21]

Recently, some researchers found that the introduction of hierarchical structures, such as re-entrant structures, marshmallow-like structures and nanoporous structures could effectively trap air, realizing superamphiphobicity.[10,22-29] Most reported surfaces are composed of re-entrant structures and marshmallow-like structures in micrometer scale, which are in the range of capillary size. Tuteja's group pioneered the study of such surface by relating the surface texture and surface chemistry to the apparent contact angle and breakthrough pressure. They constructed an ideal model with two dimensionless parameters $A^*$ and $D^*$.[10,11,30] Physically, the spacing ratio, $D^*$, is a dimensionless measure of surface porosity, which corresponds to a fraction of air trapped at the interface. The robustness factor, $A^*$, is a measure of the breakthrough pressure. A given droplet is predicted to be in the Wenzel state if $A^* \leq 1$ or in the Cassie state if $A^* > 1$. They found that the two parameters were strongly related, and optimal superamphiphobic surfaces should be designed with both $D^* \gg 1$ and $A^* \gg 1$. On the other hand, nanoporous surfaces are in the typical nanometer length scale, which maximizes the roughness of surface. For such superamphiphobic system, the length scale is small enough to

*Key Laboratory of Advanced Textile Materials and Manufacturing Technology, Zhejiang Sci-Tech University, Hangzhou 310018, China.*
*E-mail: wangsheng571@hotmail.com*
*Electronic Supplementary Information (ESI) available: Additional TGA, XPS, EDS, Nitrogen adsorption-desorption isotherm, Table of comparison of theoretical calculation of dimensionless parameters, predicted CAs, and physical structural data of the samples. See DOI: 10.1039/x0xx00000x*

prevent the transition between suspended (Cassie) to collapsed (Wenzel) wetting states. Therefore, the superamphiphobicity is attributed to the fractal nature of the nanoporous surface structure.

In the present work, we proposed a direct method to determine the relationship between structure and CA of a surface. Based on the "beads on a string" model proposed by Tuteja,[10] a series of hierarchical Te@C-$SiO_2$ nanocomposites were prepared with Te@C nanofibers as coarser texture and spherical $SiO_2$ nanoparticles (NPs) as finer texture. The nanocomposites were fluorinated and used for the fabrications of superamphiphobic film by spray-coating and for the preparation of a superamphiphobic bulk material. Considering the 80% nitrogen in the air and hierarchical structure of the nanocomposite, $N_2$ adsorption-desorption analysis was used, for the first time, to characterize the air-pockets filled in hierarchical structures and to investigate the super-repellency of the nanocomposites.

## Experimental

**Materials.** (tridecafluoro-1,1,2,2-tetrahydrooctyl)-1-trichlorosilane (Sigma Aldrich, 97%) Polyvinylpyrrolidone (PVP, MW = 58000), sodium tellurite, hydrazine hydrate (85%, w/w %), glucose, acetone, Tetraethylorthosilicate (TEOS, 98%), ethanol (AR), acetone (AR) and ammonium hydroxide (28% in water) were purchased from Sinopharm Chemical Reagent Co., Ltd. Asahiklin AK-225, was provided by Asahi Glass Co., Ltd. All of the chemical reagents were used as received.

**Fabrication of Hierarchical Structures and Surface Functionalization.** In this work, carbon coated Te nanowires (Te@C nanofibers) were used as the coarser texture, in which ultrathin Te nanowire was first synthesized via a hydrothermal method and followed by a hydrothermal carbonization procedure.[31,32] In a typical synthesis, 1.0 g of PVP, 0.09 g of sodium tellurite ($Na_2TeO_3$, 0.5 mmol), 35 mL of Mill-Q water, 1.8 mL of hydrazine hydrate and 3.2 mL of aqueous ammonia solution were added into beaker, respectively. The solution was mixed, transferred into Teflon-lined stainless steel autoclave and maintained at 180 °C for 3 h. After the autoclave was cooled to room temperature naturally, acetone was added into the obtained solution to precipitate Te nanowires, which were then centrifuged and washed several times with distilled water and ethanol. The as prepared Te nanowires were then dispersed into 50 mL of glucose solution (0.3 M) with vigorous stirring. Then the mixture was transferred into a Teflon-lined stainless steel autoclave, and maintained at 160 °C for 12 h. After being cooled down to room temperature naturally, the product (Te@C) was centrifuged, washed several times with distilled water and ethanol, and finally dried at 60 °C for 12 h.

The sol-gel process for the deposition of spherical silica NPs on nanofibers was prepared as follows. A certain amount of Te@C nanofibers was dispersed in ethanol (50 mL). Then a mixture of TEOS and ethanol (a certain amount of TEOS in 12 ml ethanol) was added into the suspension under stirring at room temperature. After reaction performed for 3 h, the obtained nanocomposites (Te@C-$SiO_2$) were washed with ethanol and water, and finally dried under vacuum (here the sample for bulk was shaped into a mold).

In order to modify nanocomposites with a superamphiphobic coating, chemical vapor deposition (CVD) of a per-fluorotrichlorosilane on the nanocomposites was performed. The nanocomposites were well crashed, and put inside a desiccator along with a glass bottle containing 40 μL of (tridecafluoro-1,1,2,2-tetrahydrooctyl)-1-trichlorosilane at 60 °C for 3 h under vacuum to obtain fluorinated nanocomposites.[12]

In the present work, Te@C nanofibers with diameters of 30, 80, 130 nm were prepared, on which $SiO_2$ nanoparticles with sizes varying from 10 ~ 50 nm were respectively in-situ deposited. The samples were denoted based on the sizes of their fibers and $SiO_2$ nanoparticles. For example, Te@C-$SiO_2$ sample containing fibers with an average diameter $R_{fiber}$ = 30 nm and $SiO_2$ nanoparticles with an average diameter $R_{particle}$ = 30 nm was denoted as F30-P30.

**Spray Coating of fluorinated nanocomposites.** Then a certain amount of the superamphiphobic nanocomposites were dispersed in AK-225 (20 g), sonicated for 30 min and then loaded into an airbrush with 0.3 mm nozzle size (Iwata Eclipse HP-CS) for spray-coating. The Operating air was controlled by the airbrush compressor at 20 psi, and the distance between the airbrush and the substrate was kept at 15 cm. After spray coating, the samples were dried in the air.

**Characterization.** The morphologies of the samples were examined with a field emission scanning electron microscope (FESEM, ZEISS VLTRA-55, Germany) at 3kV. For transmission electron microscopy (TEM) observations were obtained using a JEOL JEM-2100 instrument operating at 200 kV. Energy dispersive X-ray analysis (EDX, IncaEnergy-200) was used to investigate the sample compositions. X-ray diffraction (XRD) patterns were obtained on a D/MAX-RB X-ray diffractometer (D/Max-2550pc) using Cu-Kα radiation at a scan rate ($2\theta$) of 0.05° $s^{-1}$, and the patterns were used to determine the phase structure of the obtained samples. The accelerating voltage and the applied current were 15 kV and 20 mA, respectively. The morphology and roughness of coating surfaces were characterized by an atomic force microscope (AFM, PSIA/XE-100E) in tapping mode. The elemental analysis of the samples was carried out by X-ray photoelectron spectroscopy (XPS; Thermo Scientific K-Alpha) was used, with a monochromatized Al Kα X-ray source operated at 12 kV and 20 mA. Photoelectrons were collected at a takeoff angle of 90° relative to the sample surface. Wide-scan survey spectra were acquired using a analyzer pass energy of 100 eV and a step size of 1 eV. All binding energy values were calculated relative to the C (1s) photoelectron at 285 eV. Thermogravimetric-differential thermal analysis (TG-DTA) was performed with a Thermo plus (TG 209F3, Netzsch) instrument at a heating rate of 10 °C $min^{-1}$, while continuously supplying nitrogen at a rate of 100 mL $min^{-1}$. $N_2$ adsorption-desorption analysis of samples were conducted using a nitrogen adsorption analyzer (BeiShiDe 3H-2000BET-A, China).

The apparent contact angles (CA) of the coatings for water and oils were measured by the sessile drop method using a DSA-100 optical contact-angle meter (Kruss Company, Ltd.

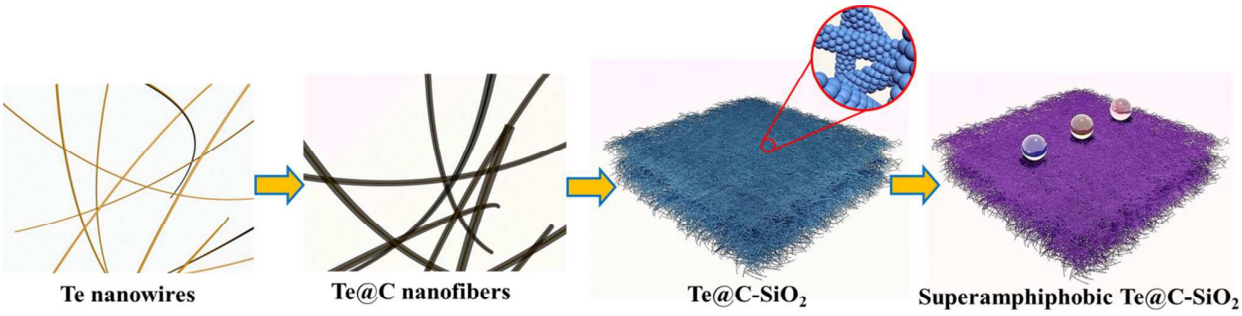


**Scheme 1.** Schematic illustration of preperation process of superamphiphobic surface.

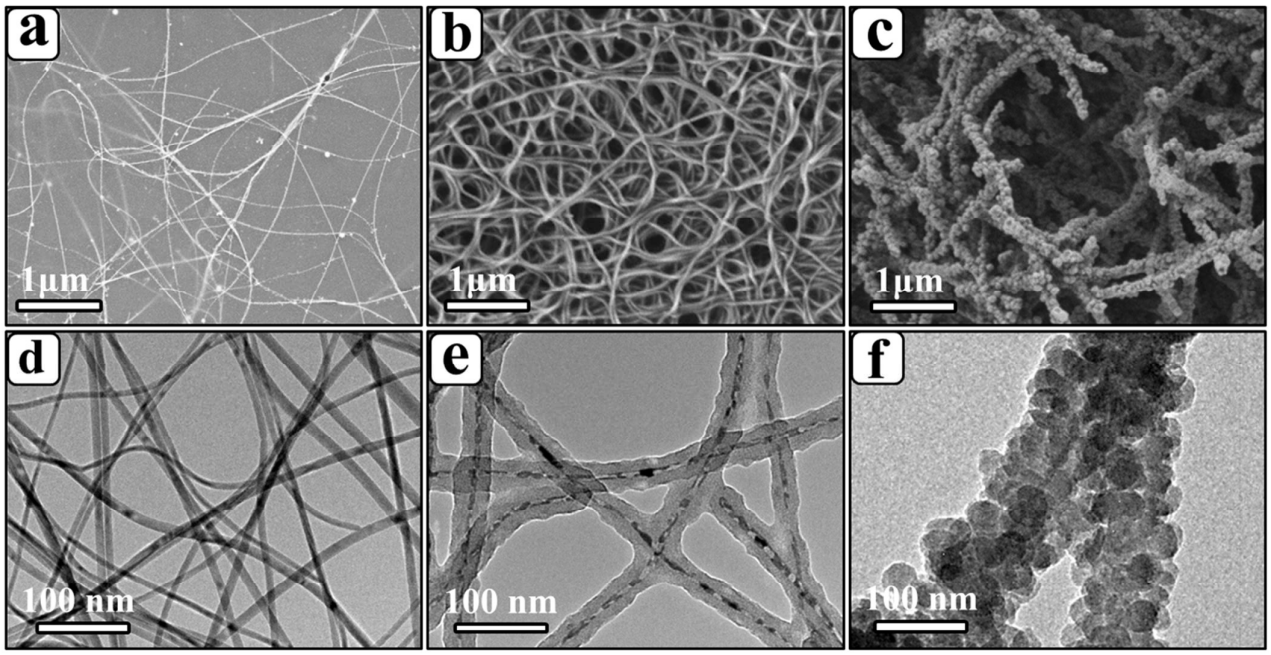


**Fig. 1** SEM images of Te nanowires (a), Te@C nanofibers, (b) Te@C-$SiO_2$ nanocomposites (F30-P30) (c) and TEM images of Te nanowires (d), Te@C nanofibers (e), Te@C-$SiO_2$ nanocomposites (F30-P30) (f).

Germany) using liquid droplets of 3 μL/2 μL (water/oil) in volume. The sliding angles (SA) were measured by a tilting stage method (BOSCH DWM40L). For each sample, the CAs and SAs were measured at 5 different positions, and the reported values represented the average of these measurements. The liquids used for contact angle measurements were droplets of deionized water, olive oil (Arawana brand, China), diiodomethane, glycerol, ethylene glycol, and *n*-hexadecane, *n*-dodecane, cyclohexane all with 99% purity, were purchased from Sigma-Aldrich

## Results and discussion

The fabrication procedure for superamniphobic nanocomposite surface, as described in the Experimental section, is schematically shown in Scheme 1. Te@C nanofibers were prepared using the method described by Yu et al.[31,32] Briefly, ultrathin high aspect ratio Te nanowires of 7 nm average diameter and several micrometers in length were first prepared (Fig. 1a and 1d) and then coated with a carbon layer by hydrothermal carbonization. The thickness of the carbon layer was precisely controlled by adjusting the reaction time. The thickness of carbon layer was set at 25 ± 2 nm at first. Its SEM image indicates that Te@C nanofibers consist of abundant randomly oriented nanofibers with a highly uniform diameter of 30 ± 2 nm and length up to hundreds of micrometers (Fig. 1b). These high aspect-ratio nanofibers were intertwisted with each other, forming a network structure. The abundant hydroxylic and carboxylic groups on the surface of Te@C nanofibers were then subjected to in-situ Stöber reaction for 3 h using TEOS as the precursor to obtain Te@C-$SiO_2$ nanocomposites (F30-P30). As shown in Fig. 1c and 1f, the original twisted fibers were straightened and spherical silica NPs with uniform size (of ~ 30 nm) completely covered the surface of each Te@C nanofiber. The in-situ deposition of $SiO_2$ NPs resulted in a nanoscale roughness (finer texture) on the nanofiber surface (coarser texture), forming a hierarchical structure at same length level. The superhydrophilicity of the Te@C-$SiO_2$ nanocomposites to water and oil was confirmed with the profile of water and *n*-hexadecane droplets (Supporting Information S1). TGA

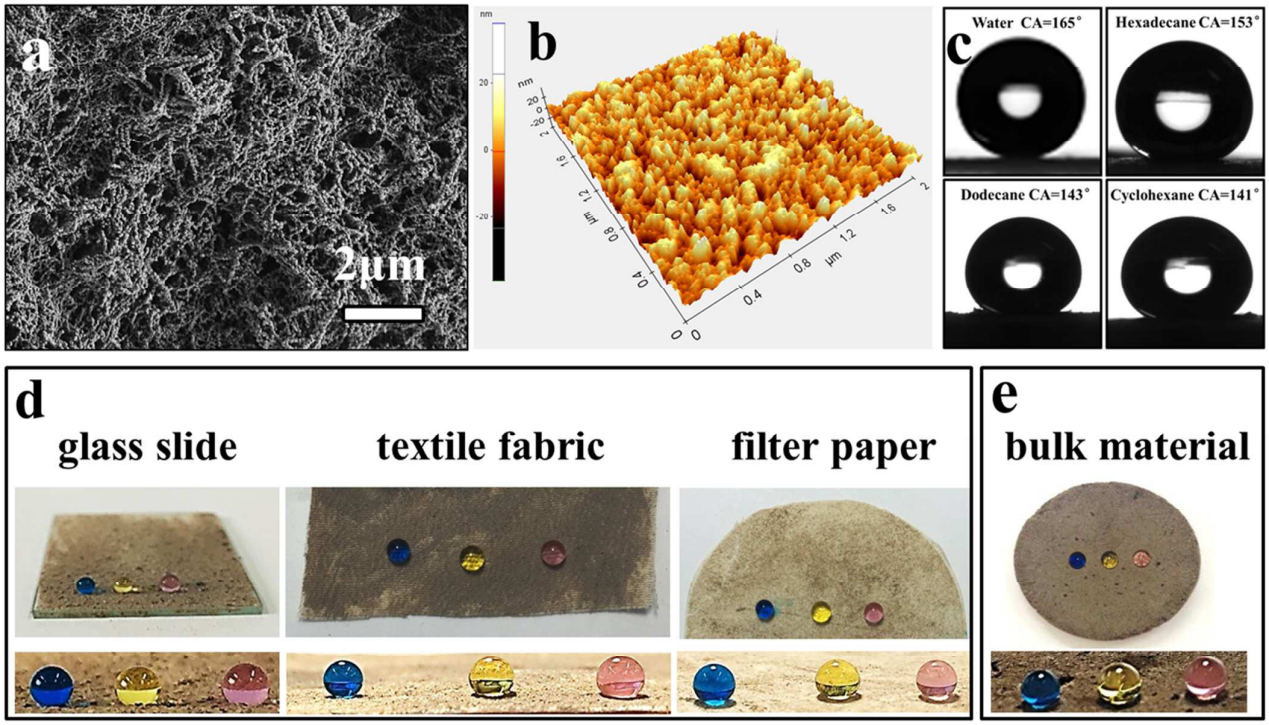


**Fig. 2** (a) and (b) the selected SEM and AFM images of fluorinated Te@C-$SiO_2$ nanocomposites; (c) Profile photographs of water, *n*-hexadecane, *n*-dodecane and cyclohexane on fluorinated Te@C-$SiO_2$ nanocomposites; (d) Digital photographs of droplets of water, olive oil and *n*-hexadecane on Te@C-$SiO_2$ coated glass slide, fabric and filter paper; (e) Droplets on shaped Te@C-$SiO_2$ bulk material. Blue droplets: water (dyed with methylene blue); yellow droplets: oliver oil and pink droplets: *n*-hexadecane (dyed with disperse red 3B).

analysis indicates that the loading amount of $SiO_2$ nanoparticles of was ~ 8.1% (Supporting Information S2).

The surface of Te@C-$SiO_2$ nanocomposites were then fluorinated with perfluorotrichlorosilane, dispersed into AK225 and spay-coated on a substrate. The chemical compositions of Te nanofibers, Te@C, Te@C-$SiO_2$ and florinated Te@C-$SiO_2$ were analyzed with EDS (Supporting Information S3) and their chemical states were determined with an X-ray photoelectron spectroscopy (XPS) measurements. It is clear that the signal of fluorine was found at 688.26 eV in the survey spectrum of the flluorinated Te@C-$SiO_2$ nanocomposite (Supporting Information S4), indicating the successful fluorination.

To determine the effects of the fluorination, fluorinated Te@C-$SiO_2$ nanocomposite was spray-coated on various substrates and characterized. Fig. 2a and 2b show the SEM and AFM images of the spray-coated surface of fluorinated F30-P30. In addition, the fluorinated F30-P30 was also shaped as bulk superamphiphobic material due to its flexibility (Fig. 2d and 2e, Movie S1, S2). It can be seen that no significant morphology change was found after the fluorination (Fig. 1c vs Fig. 2a). The droplets of water and *n*-hexadecane, *n*-dodecane and cyclohexane formed a nearly spherical liquid droplet on the fluorinated F30-P30 coated glass slide (Fig. 3c). Particularly, CAs of water and n-hexadecane reached 165° and 153°, respectively. The Te@C-$SiO_2$ nanocomposite coatings on

**Table 1.** CAs and SAs of liquids with different surface tensions on the fluorinated Te@C-$SiO_2$ coated glass slides.

| liquid | Surface tension [mN $m^{-1}$] | CA [°] | SA [°] |
|---|---|---|---|
| Water | 72.1 | 165 ± 1 | 0.1 ± 0.1 |
| glycerol | 64.0 | 161 ± 1 | 0.5 ± 0.1 |
| Diiodomethane | 50.9 | 159 ± 1 | 1.0 ± 0.1 |
| Ethylene glycol | 47.3 | 158 ± 1 | 1.3 ± 0.1 |
| Olive oil | 32.0 | 156 ± 1 | 2.9 ± 0.1 |
| *n*-Hexadecane | 27.5 | 153 ± 1 | 4.2 ± 0.1 |
| *n*-Dodecane | 25.3 | 145 ± 1 | 7.0 ± 0.2 |
| Cyclohexane | 24.9 | 141 ± 1 | 9.2 ± 0.2 |

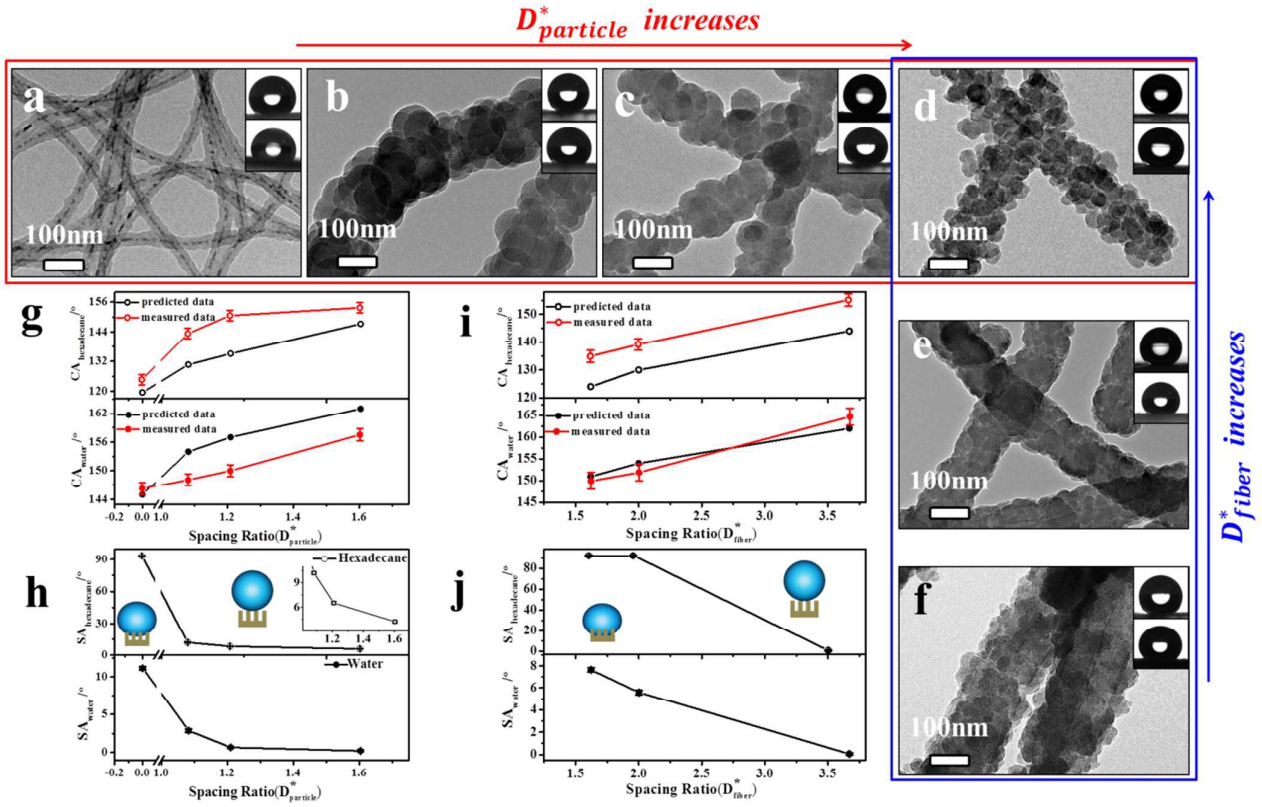


**Fig. 3** (a), (b), (c) and (d) are the SEM images of the hierarchically structured samples F30-P0, F30-P50, F30-P40 and F30-P30 with a particle spacing ratio $D^*_{particle}$ = 0, 1.1, 1.2, 1.6, respectively. (d), (e) and (f) are the SEM images of the hierarchically structured samples F30-P30, F80-P30 and F130-P30 with a fiber spacing ratio $D^*_{fiber}$ = 3.7, 2.0, 1.6, respectively. (g) and (h) are the apparent contact angles and the sliding angles, respectively, as a function of the particle spacing ratio for *n*-hexadecane and water. (i) and (j) show the apparent contact angles and the sliding angles, respectively, as a function of the fiber spacing ratio for *n*-hexadecane and water, respectively. The insets are the profile of water (upper) and *n*-hexadecane (lower) on the surface.

textile fabric and paper and its bulk material showed similar superamphiphobicity. Table 1 shows the summary of the CA and SA values of some typical liquids with different surface tensions on the spray-coated glass slide. The CAs of all liquids with more polarities than *n*-hexadecane are higher than 150°, and their SAs are lower than 5°, indicating the excellent superamphiphobicity of the surface. The CAs of both *n*-dodecane and cyclohexane are lower than 150° and their SAs are higher than 5°, suggesting the transformation from the Cassie state to the metastable state between the Wenzel and the Cassie states. The superamphiphobicity of the fluorinated Te@C-$SiO_2$ nanocomposite coatings can be attributed to the surface with hierarchical structures and the fluoroalkyl groups.

Considering the significant effects of surface roughness on super-repellency, Tuteja et al. proposed two dimensionless parameters $D^*$ and $A^*$.[10,11,30] The spacing ratio, $D^*$, corresponds to a fraction of air trapped at the interface and the robustness factor, $A^*$, is a measure of the breakthrough pressure. They demonstrated that the two parameters are strongly related, and optimal superamphiphobic surfaces should be designed with both $D^* \gg 1$ and $A^* \gg 1$.

According to the "beads on a string" model proposed by Tuteja (Supporting Information S5),[11,20] the hierarchical roughness of Te@C-$SiO_2$ is related to the dual scale structure, the coarser texture derived from Te@C fibers ($D^*_{fiber}$) and the finer texture from close packed spherical $SiO_2$ NPs. We then systematically investigated the effects of finer/coarser texture on the apparent contact angles ($\theta^*$) of water and *n*-hexdecane, respectively.

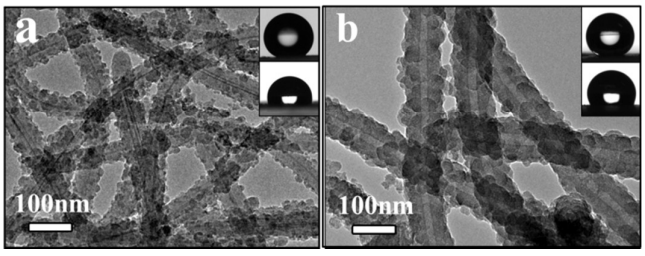


**Fig. 4** (a) and (b) are the SEM images of the hierarchical F30-P10 and F30-P20, respectively. The insets are the profile images of the water droplet (upper) and hexadecane droplet (lower) on the corresponding surfaces.

**Table 2.** Values of the dimensionless parameters, and predicted CA.

| Sample | $R_{particle}$ (nm) | $D_{particle}$ (nm) | $D^*_{particle}$ | $A^*_{Hierarchical}$ water/hexadecane | CA $_{predicted}$ /° water/hexadecane | CA $_{measured}$ /° water/hexadecane | SA $_{measured}$ /° water/hexadecane |
|---|---|---|---|---|---|---|---|
| **F30-P0** | 0 | 0 | NA | 17054 / 13363 | 142.9 / 127.4 | 147 ± 2 / 125 ± 2 | 10 ± 0.2 / NA |
| **F30-P50** | 25 | 1 | 1.082 | 22565 / 8208 | 154.3 / 129.3 | 150 ± 2 / 143 ± 2 | 2.5 ± 0.2 / 10.2 ±0.2 |
| **F30-P40** | 20 | 2 | 1.210 | 23755 / 9453 | 156.4 / 133.9 | 153 ± 2 / 150 ± 2 | 0.5 ± 0.1 / 6.5 ± 0.2 |
| **F30-P30** | 15 | 4 | 1.604 | 26548 / 12243 | 161.5 / 143.4 | 165 ± 2 / 153 ± 2 | 0.1 ± 0.1 / 4.2 ± 0.2 |
| **Sample** | $R_{fiber}$ (nm) | $D_{fiber}$ (nm) | $D^*_{fiber}$ | $A^*_{Hierarchical}$ water/hexadecane | CA $_{predicted}$ /° water/hexadecane | CA $_{measured}$ /° water/hexadecane | SA $_{measured}$ /° water/hexadecane |
| **F130-P30** | 65 | 40 | 1.62 | 51657 / 2825 | 151 / 123.6 | 151±2 / 134±2 | 7.0±0.2 / NA |
| **F80-P30** | 40 | 40 | 2.0 | 44196 / 4591 | 154 / 129.7 | 153±2 / 138±2 | 5.0±0.2 / NA |
| **F30-P30** | 15 | 40 | 3.67 | 26548 / 12243 | 161.5 / 143.4 | 165±2 / 153±2 | 0.1±0.1 / 4.2±0.2 |
| **Sample** | $R_{particle}$ (nm) | $D_{particle}$ (nm) | $D^*_{particle}$ | $A^*_{Hierarchical}$ water/hexadecane | CA $_{predicted}$ /° water/hexadecane | CA $_{measured}$ /° water/hexadecane | SA $_{measured}$ /° water/hexadecane |
| **F30-P10** | 5 | 10 | 9 | 98684 / 37144 | 176 / 169 | 152 ± 2 / 111 ± 2 | 6.2 ± 0.2 / NA |
| **F30-P20** | 10 | 10 | 4 | 75878 / 29441 | 170 / 162 | 155 ± 2 / 121 ± 2 | 4.7 ± 0.1 / NA |

A series of Te@C-$SiO_2$ nanocomposites ($D^*_{particle}$) including F30-P0, F30-P50, F30-P40 and F30-P30 with a fixed $\boldsymbol{D^*_{fiber}}$ of 3.67 ($R_{fiber}$ = 15 ± 2 nm) and various $D^*_{particle}$ (Fig. 3 a-d, Table 1 in Supporting Information S6) were prepared and used to study the influence of the finer texture on CA. F30-P0 was prepared by coating a $SiO_2$ layer on Te@C to completely eliminate the influence of the organic functional groups of outside carbonaceous layer and used as a reference sample (Fig. 3a, $D^*_{particle}$ = 0, coarser texture). $D^*_{particle}$ of nanocomposites F30-P50, F30-P40 and F30-P30 are shown in in Fig. 3b, 3c and 3d. No super-repellency was observed on F30-P0 with coarser texture alone. The sample surface showed a superhydrophobicity and metastable state for *n*-hexdecane droplet with increase of $D^*_{particle}$ to 1.2 ($R_{particle}$ = 25 ± 2 nm and 20 ± 2 nm). As $D^*_{particle}$ increased to 1.6 ($R_{particle}$ = 15 ± 2 nm), the sample surface showed superamphiphobicity.

The influence of the coarser texture on CAs was investigated with composites F30-P30, F80-P30 and F130-P30. These composites were prepared with a fixed $D^*_{particle}$ ($R_{particle}$ = 15 ± 2 nm) and various $D^*_{fiber}$, ranging from 1.6 to 3.67 ($R_{fiber}$ = 65 ± 2 nm to 15 ± 2 nm) (Table 2 in Supporting Information S6). As can be seen, *n*-hexadecane was in Wenzel state on both F80-P30 and F130-P30 spray-coated slides. The composites coated surface only showed superamphiphobicity as $D^*_{fiber}$ increased into 3.7 ($D^*_{fiber}$ = 3.7, $R_{fiber}$ = 15 ± 2 nm).

$A^*$ can be calculated with equation 7 (Supporting Information S5) with respect to $D^*_{fiber}$ and $D^*_{particle}$. As shown in Table 2, for all above systems, $A^* \gg 1$. Excellent superamphiphobicity was achieved when $A^*$= 12243, at the highest $D^*$ value ($D^*_{fiber} = 3.67$, $D^*_{particle} = 4$), consistent with the conclusion of Tuteja.

However, continuously increasing $A^*$ and $D^*$ led to the transition from the Cassie state to the Wenzel state back (F30-P10, F30-P20), which could not be explained by the design chart (Table 2 and Fig. 4a and 4b). Both F30-P10 and F30-P20 composites had extremely high $D^*_{particle}$ and $A^*_{particle}$, but showed poor oleophobicity.

Both fibers and nanoparticles of the "beads on a string" system were in nanoscale, which lead to a very high $A^*$. Therefore, the breakthrough pressure from capillary force of such system is no longer the main reason for the transition from the Cassie state to the Wenzel state. Based on the porous characteristics of nanomaterials, stable hierarchical structure of the sprayed Te@C-$SiO_2$ nanocomposites, and the composition of the air, we characterized the air-pockets with $N_2$ adsorption-desorption isotherms and for the first time attempted to relate the $S_{BET}$ of the material to the wettability of the surface.

Fig. 5a-d are the nitrogen adsorption-desorption isotherms of the sample F30-P0, F30-P50, F30-P40 and F30-P30 (Fig. 3a-d). Their relevant BET specific surface areas ($S_{BET}$) of the samples are displayed in the insets of the corresponding figures. As can be seen, All samples showed typical type IV adsorption isotherms with H3-type hysteresis loops according to BDDT classification, indicating they contain both mesopores (2-50 nm) and macropores (> 50 nm). Fig. 5e-h show their pore size distributions, respectively. As a reference sample, F30-P0 showed a similar $S_{BET}$ to that of Te@C nanofibers (Supporting Information S6). It exhibited a wide pore size distribution

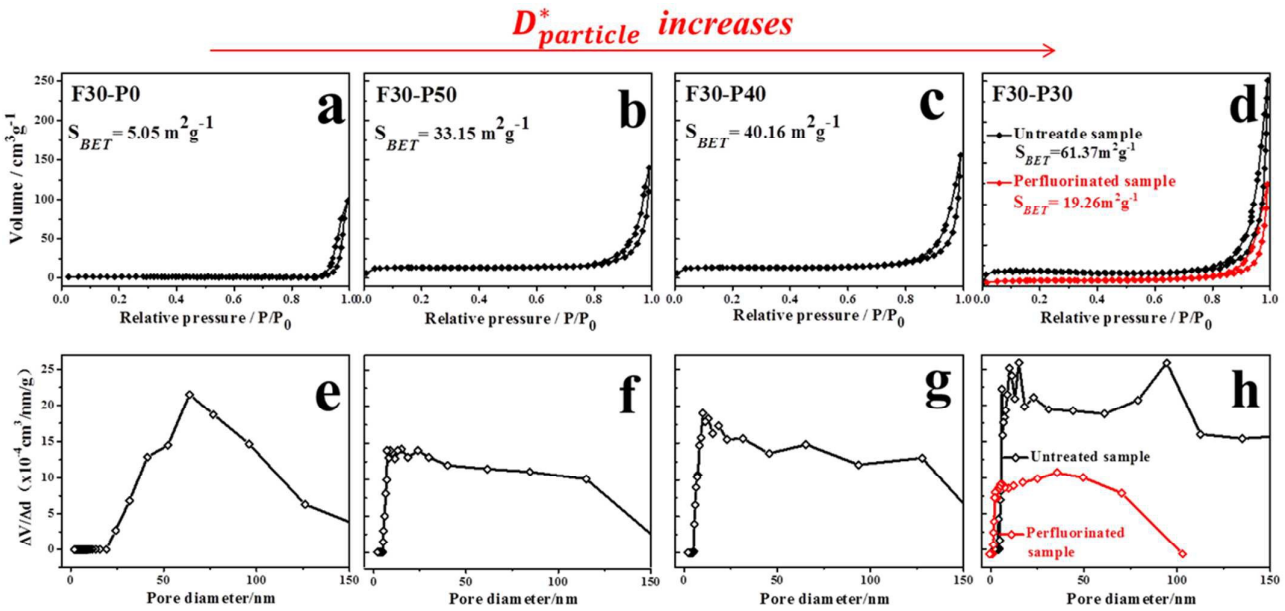


Fig. 5 (a), (b), (c) and (d) are the Nitrogen adsorption-desorption isotherms of F30-P0, F30-P50, F30-P40 and F30-P30 with $D^*_{particle}$ of 0, 1.1, 1.2 and 1.6, respectively. Their corresponding pore size distributions from the adsorption branch are shown in (e), (f), (g) and (h), respectively.

ranging from ~20 to 200 nm and was mainly composed of macropores with average pore size at 72 nm that was attributed to the porosity of coarser texture.

When $SiO_2$ nanoparticles in-situ grew on the Te@C, finer texture was introduced into system, leading to a dramatic increase in $S_{BET}$. Particularly, F30-P30 with excellent superamphiphobicity showed the highest $S_{BET}$ value, which is ten times higher that of F30-P0. Compared with sample F30-P0 that only had coarser texture, all other nanocomposites with hierarchical structures including F30-P50, F30-P40 and F30-P30 showed increased amounts of mesopores with size ranging from 5 to 50 nm, which is mainly due to the porosity of the finer texture of in-situ loaded $SiO_2$ NPs.

Interestingly, $S_{BET}$ and the pore number of fluorinated F30-P30 was significantly decreased (red line in Fig. 5d and 5h). The reduced pore number indicates the successful surface modification, which effectively prevented access of $N_2$ and significantly reduced the $N_2$ adsorption/desorption. In addition, the results indicate that the chemical modification is beneficial to the air-trap on the hierarchical surface.

Fig. 6 shows the nitrogen adsorption-desorption isotherms of the composites with various $\boldsymbol{D^*_{fiber}}$ (Fig. 3d-f) and their pore size distributions. It is obvious that SBET of Te@C-$SiO_2$ composites is rapidly decreased with the increase of fiber size from 30 nm to 130 nm. It can be explained that proportion of macropores is gradually increased with the increase of fiber size that is the major contribution to $S_{BET}$, leading to a significant decrease in $S_{BET}$. It can be seen there is almost no difference between F80-P30 and F130-P30 in the number of mesopores, while the later show significant increase in the number of macropores.

Finally, $N_2$ adsorption-desorption analysis was conducted on F30-P10 and F30-P20 (Fig. 7). It is worth noting both of them showed much high $S_{BET}$, and among all nanocomposites, F30-P10 exhibited highest $S_{BET}$. In addition, F30-P10 and F30- P20 were mainly composed of large number of micropores with size lower than 10 nm, which far exceeds that of macropores.

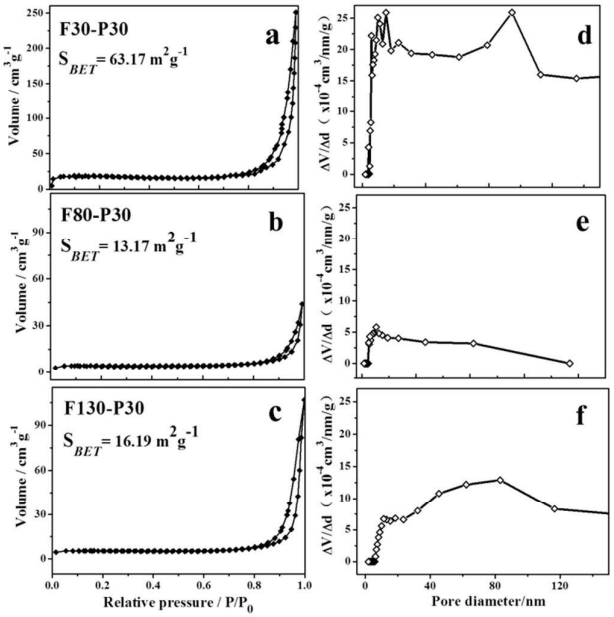


Fig. 6 (a), (b) and (c) are nitrogen adsorption-desorption isotherms of F30-P30, F80-P30 and F130-P30 with $D^*_{fiber}$ of 3.7, 2.0 and 1.6, respectively. Their pore size distributions from the adsorption branch are shown in (d), (e) and (f), respectively.

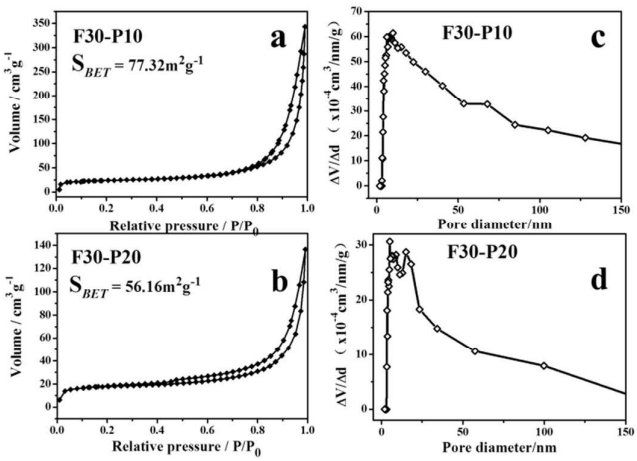


Fig. 7 (a) and (b) are the nitrogen adsorption-desorption isotherms of F30-P10 and F30-P20, respectively. Their pore size distributions from the adsorption branch are shown in (c) and (d), respectively.

It is well known that the wetting behaviour of a liquid on a solid substrate can be determined by the difference between the cohesive interaction that holds the liquid together and the adhesive interaction between the liquid and the solid.[33,34] The air-pockets trapped in the texture can reduce the contact area between the liquid and the surface, especially in Cassie state, which consequently reduces the adhesive interaction ($\boldsymbol{\cos\theta^* = f_1\cos\theta - f_2}$, when $f_1$<<1, the repellency is increased significantly) and, increases the repellency and roll-off of the droplets on the surface.[35] For example, a hydrophobic perfluoroalkyl modified smooth $SiO_2$ surface of $SiO_2$ particles is still highly adhesive (Supporting Information S5), indicating the contact between a liquid and solid phases is governed by adhesive interaction. The surface anti-wettability can be significantly enhanced with surface structures, such as micro, nano, and micro/nano, were introduced. If the three structured surfaces (micro, nano, and micro/nano) show similar CAs to a liquid droplet, for a micro-structured surface, the area fraction of the liquid/solid interface is greatly decreased due to the involvement of micro air-pockets. However, it has been demonstrated that such micro air-pockets can be easily penetrated due to the capillarity effect, producing a high SA. Since the nano-structured surface can bring large amounts of nano-scale air-pockets and has a robust repellency,[36] it can effectively prevent such penetration. However, the dense solid contact points between the liquid and nano-structured surface are significantly increased, leading to a large area fraction of the liquid/solid interface and thus stronger adhesive interactions. Therefore, high SA is sometime inevitable, especially for those liquid with lower surface energy. Micro/nano structured surface can overcome these disadvantages of both single textured surfaces to achieve the smallest adhesive interaction.[20,37] It has been demonstrated that the adhesive interaction follows the order of smooth structured surface > micro-structured surface > nano-structured surface > micro/nano- structured (hierarchically structured) surface.[37]

As discussed in our work, all Te@C-$SiO_2$ nanocomposites exhibited unique porous structures and $S_{BET}$ and pore size distributions, leading to different CAs and SAs. To avoid confusion, the air-pockets produced by "beads on a string" nanocomposites and BET analysis, that is, macropores of coarser texture were denoted as macro air-pockets (> 50 nm) and the mesopores of the finer texture were denoted as micro air-pockets (< 50 nm).

As can been seen, no desired super-repellency can be obtained for micro-structured sample F30-P0 with a single textured surface that mainly consists of macro air-pockets (water was in a metastable state and *n*-hexadecane was completely in Wenzel state). In contrast, nano-structured sample P30 (reference sample in Supporting Information S7) that exhibited very high $S_{BET}$ and significantly centralized size distribution in mesoporous region, showed enhanced performance (water was in excellent Cassie state and *n*-hexadecane was completely in Wenzel state). However, the nano-structured surface still showed poor repellency to *n*-hexdecane, which may be due to the above mentioned stronger adhesive interactions derived from extremely lower surface energy of *n*-hexadecane. The limited oleophobicity of single textured surface also can be confirmed in our study.

As described above, a micro/nano structured surface can balance the number of air-pockets and area fraction of liquid/solid interface, achieving the smallest adhesive interactions (Fig. 4c). Nanocomposites including F30-P30, F30-P40, F30-P50 and F80-P30 showed dual hierarchical structure with similar pore size distribution shapes, suggesting that each nanocomposite had same amounts of air-pockets within all size range (≥ 5 nm). Their different amounts of air-pockets lead to different $S_{BET}$ and air volume (Supporting Information S9). Due to their dual hierarchical structure, all nanocomposites showed excellent superhydrophobicity, but different oleophobicity that increased with their $S_{BET}$ from Wenzel state (F80-P30) to metastable state (F30-P50 and F30-P40) to Cassie state (F30-P30). F30-P30 showed excellent superamphiphobicity, the highest $S_{BET}$, and number of macro/micro air-pockets, indicating that its superamphiphobicity is exactly the structurally enhanced hydrophobicity. This is the first time to relate the Cassie state with the air-pockets trapped in material itself. The concept "micro/nano air-pockets", should be a very unique "continuous and balance state" for all air-pockets involved in hierarchical structure.

Finally, unlike the nanocomposites discussed above, F30-P10, F30-P20 and F130-P30 also showed dual hierarchical structure, but poor repellency to oil (completely Wenzel state). This might be attributed to uniformity of their size distributions in mesopores or macropores, which are highly localized in either mesopore or macropore regions. Such size distributions are very similar to that of single textured nanocomposites (P30 and F30-P0). It is considered such significant dominance of distribution of macro-air pockets or micro-air pockets is the reason to lead to the poor oleophobicity.

## Conclusions

In summary, based on the "beads on a string" model, a series of hierarchical Te@C-$SiO_2$ nanocomposites were prepared with Te@C nanofibers as coarser texture and spherical $SiO_2$ nanoparticles (NPs) as finer texture. The Te@C-$SiO_2$ nanocompoiste was fluorinated with perfluorotrichlorosilane to obtained superamphiphobicity. The fluorinated Te@C-$SiO_2$ was used for spray-coating on various substrates and the preparation of bulk material. $N_2$ adsorption-desorption analysis was for the first time used to characterize the air-pockets trapped in hierarchical structures. The results indicate that superamphiphobicity was attributed to the synergistic effect of the micro-scale structure and the nano-scale structure. Excess of either of the textures can reduce the superamphiphobicity. The air-pockets of the super-repellent "beads on a string" materials possess the following features: higher $S_{BET}$ that ensures enough air-pockets ($S_{BET}$ of superamphiphobic sample is much higher than that of superhydrophobic one); and the most important, continuous and balanced size distribution of micropores and macropores derived from hierarchical structure.

The hierarchical structures with significant size distribution in the range of coarser or finer texture behaved like the surface structure of single texture. For such surface, various successful superamphiphobic surfaces suggested that the modification with the lowest surface energy material such as fluorodecyl POSS ($\gamma_{SV}$ = 10 mN/m) may reduce adhesive interactions to achieve superwettabilty.[30,38]

In full, a new method was proposed to understand the Cassie state on "beads on a string" materials. The method can be considered as a simple evaluation method for the wettability of materials with nanoscale hierarchical structures. Superamphiphobicity is still not well understood, we expect the method will deepen and broaden the field.

## Acknowledgements

We thank the National Natural Science Foundation of China (NO. 51471153 and 51372227), Natural Science Foundation of Zhejiang province (NO. LY14E020011) and 521 Talent Project of Zhejiang Sci-Tech University for providing financial support.

## Notes and references

1 W. Barthlott and C. Neinhuis, *Planta* 1997, **202**, 1-8.
2 C. Neinhuis and W. Barthlott, *Ann. Bot.* 1997, **79**, 667-677.
3 K. S. Liu, M. Y. Cao, A. Fujishima and L. Jiang, *Chem. Rev.* 2014, **114**, 10044-10094.
4 M. Wolfs, T. Darmanin and F. Guittard, *Polym. Rev.* 2013, **53**, 460-505.
5 X. Li, D. Reinhoudt and M. Crego-Calama, *Chem. Soc. Rev.* 2007, **36**, 1350-1368.
6 M. Liu, Y. Zheng, J. Zhai and L. Jiang, *Acc. Chem. Res.* 2010, **43**, 368-377.
7 X. Feng and L. Jiang, *Adv. Mater.* 2006, **18**, 3063-3078.
8 H-J. Butt, I. V. Roisman, M. Brinkmann, P. Papadopoulos and D. Vollmer, *Current Opinion in Colloid and Interface Science* 2014, **19**, 343-354.
9 S. Herminghaus, *Europhys Lett* 2000, **52**, 165-170.
10 A. Tuteja, W. Choi, M. Ma, J-M. Mabry, S-A. Mazzella, G-C. Rutledge, G-H. Mckinley and R-E. Cohen, *Science* 2007, **318**, 1618-1622.
11 A. Tuteja, W. Choi, J-M. Mabry, G-H. McKinley and R-E. Cohen, *Proc. Natl. Acad. Sci. U.S.A.* 2008, **105**, 18200-18205.
12 X. Deng, F. Schellenberger, P. Papadopoulos, D. Vollmer and H-J. Butt, *Langmuir* 2013, **29**, 7847-7856.
13 T. S. Wong,; S. H. Kang, K. Y. Tang, E. J. Smythe, B. D.Hatton, A. Grinthal and J. Aizenberg, *Nature* 2011, **477**, 443-447.
14 K. Liu, Y. Tian and L. Jiang, *Prog. Mater. Sci.* 2013, **58**, 503-564.
15 H. Wang, H. Zhou, A. Gestos, J. Fang and T. Lin, *ACS Appl. Mater. Interfaces* 2013, **5**, 10221-10226.
16 H. Zhao, K-Y. Law and V. Sambhy, *Langmuir* 2011, **27**, 5927-5935.
17 M. Im, H. Im, J. H. Lee, J. B. Yoon and Y. K. Choi, *Soft Matter* 2010, **6**, 1401-1404.
18 A. Ahuja, J. A. Taylor, V. Lifton, A. A. Sidorenko, T. R. Salamon, E. J. Lobaton, P. Kolodner and T. N. Krupenkin, *Langmuir* 2008, **24**, 9-14.
19 X. Gao and L. Jiang, *Nature* 2004, **432**, 36.
20 A. K. Kota, G. Kwon and A. Tuteja, *NPG Asia Materials* 2014, **6**, 1-16.
21 L. Wen, Y. Tian and L. Jiang, *Angew. Chem. Int. Ed.* 2015, **54**, 3387-3399.
22 R. Hensel, R. Helbig, S. Aland, H-G. Braun, A. Voigt, C. Neinhuis and C. Werner, *Langmuir* 2013, **29**, 1100-1112.
23 L. Joly and T. Biben, *Soft Matter* 2009, **5**, 2549-2557.
24 R. Almeida and J. W. Kwon, *Langmuir* 2013, **29**, 994-998.
25 H. Zhao, K. C. Park and K. Y. Law, *Langmuir* 2012, **28**, 14925-14934.
26 X. Deng, L. Mammen, H. J. Butt and D. Vollmer, *Science* 2012, **335**, 67-70.
27 V. A. Ganesh, S. S. Dinachali, A. S. Nair and S. Ramakrishna, *ACS Appl. Mater. Interfaces* 2013, **5**, 1527-1532.
28 D. Ge, L. Yang, Y. Zhang, Y. Rahmawan and S. Yang, *Part. Part. Syst. Charact.* 2014, **31**, 763-770.
29 T. C. Rangel, A. F. Michels, F. Horowitz and D. E. Weibel, *Langmuir* 2015, **31**, 3465-3472.
30 A. K. Kota, Y. Li, J. M. Mabry and A. Tuteja, *Adv. Mater.* 2012, **24**, 5838-5843.
31 H-W. Liang, L. Wang, P-Y. Chen, H-T. Lin, L-F. Chen, D. He and S-H. Yu, *Adv. Mater.* 2010, **22**, 4691-4695.
32 H-W. Liang, W-J. Zhang, Y-N. Ma, X. Cao, Q-F. Guan, W-P. Xu and S-H. Yu, *ACS NANO* 2011, **5**, 8148-8161.
33 D. Bonn, J. Eggers, J. Indekeu, J. Meunier and E. Rolley, *Rev. Mod. Phys.* 2009, **81**, 739-805.
34 H. Bellanger, T. Darmanin, E. T. de-Givenchy and F. Guittard, *Chem. Rev.* 2014, **114**, 2694-2716.
35 A. B. D. Cassie and S. Baxter, *Trans. Faraday Soc.* 1944, **40**, 546-551.
36 A. Checco, B. M. Ocko, A. Rahman, C. T. Black, M. Tasinkevych, A. Giacomello and S. Dietrich, *Physical Review Letters* 2014, **112**, 216101-216105.
37 P. Zhang, S. Wang, S. Wang and L. Jiang, *small* 2015, **11**, 1939-1946.
38 H. Wang, H. Zhou, A. Gestos, J. Fang and T. Lin, *ACS Appl. Mater. Interfaces* 2013, **5**, 10221-10226.